Journal of Marine Science and Technology

Volume 30 | Issue 2 Article 2

Variance of TD-Mosaic Dual-Vortex Interactions Between In-Fa and Cempaka (2021) in the North Pacific

Tsorng-Lin Chia
Department of Computer and Communication Engineering, Ming Chuan University, Taoyuan, Taiwan 333, R.O.C.,
tlchia@mail.mcu.edu.tw

Guang-Yang Pan
School of Data and Computer Science, Guangdong Peizheng College, Guangzhou, Guangdong Province, People's Republic of China

Ji-Chyun Liu
Department of Computer and Communication Engineering, Ming Chuan University, Taoyuan, Taiwan 333, R.O.C

Recommended Citation

Chia, Tsorng-Lin; Pan, Guang-Yang; and Liu, Ji-Chyun (2022) "Variance of TD-Mosaic Dual-Vortex Interactions Between In-Fa and Cempaka (2021) in the North Pacific," *Journal of Marine Science and Technology*: Vol. 30: Iss. 2, Article 2.
DOI: 10.51400/2709-6998.2569
Available at: https://jmstt.ntou.edu.tw/journal/vol30/iss2/2

Variance of TD-Mosaic Dual-Vortex Interactions Between In-Fa and Cempaka (2021) in the North Pacific

Acknowledgements

This work was supported in part by the Ministry of Science and Technology (MOST), through MOST grant 110-2221-E-130-006.

RESEARCH ARTICLE

Variance of TD-Mosaic Dual−Vortex Interactions Between In-Fa and Cempaka (2021) in the North Pacific

Tsorng-Lin Chia [a,*], Guang-Yang Pan [b], Ji-Chyun Liu [a]

[a] Department of Computer and Communication Engineering, Ming Chuan University, Taoyuan 333, Taiwan, R.O.C
[b] School of Data and Computer Science, Guangdong Peizheng College, Guangzhou, Guangdong Province, People's Republic of China

Abstract

A study of the different types of dual-vortex interactions or "Fujiwara effects" between two storms is crucial for considerably improving weather forecasts. This study combined remote sensing images, empirical formulas based on the possibility of storm interaction (Liou−Liu formula), and vector addition techniques to accurately analyze In-Fa and Cempaka typhoons and the surrounding weather patterns during the 2021 typhoon season in the North Pacific. Although the distance separating the typhoons In-Fa and Cempaka was 1,800−2,040 km, the influence of middle air flow and a tropical depression (TD) caused a "vector superposition TD-mosaic double-vortex" interaction between the two typhoons. Therefore, this paper proposes a new dual-vortex interaction between the typhoons studied here. This newly discovered interaction is different from the normally observed double-vortex interaction between storms. In the same context, these interactions caused strong typhoons with eye diameters of 20, 25, 55, 60, 65, 75, and 100 km and led to the turning and U-turn trajectories of the typhoons In-Fa and Cempaka. This paper uses linear (vector) space technology, namely vector addition diagrams, to describe the vector addition TD-mosaic double-vortex interaction between tropical cyclones and TDs.

Keywords: Fujiwhara effect, Vortex interaction, Liou−Liu formulas, Vector addition TD-mosaic dual-vortex

1. Introduction

Accurate prediction of the migratory track, intensity, and rainfall of tropical cyclones (TCs) is a crucial research focus for meteorologists and weather forecasters [1]. Factors influencing track orientation, track shape, track sinuosity, and ultimately, landfall points are of particular interest [2,3]. Satellite-based cloud images can be used to analyze the TC cloud structure and dynamics [4−8].

Concurrent with climatic variability and global warming in recent decades, an increasing number of dual-TC formations has been noted in various ocean basins. A recent review detected 10 dual-vortex interactions in the Northwest Pacific (NWP) within just 5 years (2013−2017) [9]. The conventional "Fujiwhara effect," also referred to as Fujiwhara interaction, binary interaction, or dual-vortex interaction, occurs between any two TC systems that are less than 1,400 km apart, with mutual effects on the strength and direction. The behavior patterns of such interactions can be classified as complete merge (CM), partial merge (PM), complete straining out (CSO), partial straining out (PSO), and elastic interaction (EI) [10,11]. EI is frequently associated with changes in the track direction and the execution of complex/looping tracks. Occasionally, typhoons execute a U-turn with increasing intensity. Analyzing the different types of dual-vortex interactions is critical for improving future weather forecasts, as the Fujiwhara effect is yet to be

Received 13 October 2021; revised 12 November 2021; accepted 22 February 2022.
Available online 17 May 2022.

* Corresponding author.
E-mail addresses: tlchia@mail.mcu.edu.tw (T.-L. Chia), dranyu@qq.com (G.-Y. Pan), jchyunliu@gmail.com (J.-C. Liu).

https://doi.org/10.514/2709-6998.2569

incorporated into climate models. This paper introduces a newly detected dual-vortex interaction referred to as "vector addition leakage (VAL)." Regarding dual-vortex interactions, a key example is the dual-vortex interactions between typhoons Melor and Parma in the NWP basin, which caused unexpected heavy damage over the Philippines in 2009 and considerable errors in prediction [12]. Several such dual-vortex interactions have been studied in the past [9−15]. For instance, Hart and Evans [16] simulated the interaction of dual vortices in horizontally sheared environmental flows on a beta plane, and Galarneau et al. [17] investigated the intensification of Hurricane Sandy in 2012 during the warm seclusion phase of its extratropical transition.

Indirect dual-vortex interactions between any two TCs through another mid-lying weaker tropical storm (TS) or tropical depression (TD) have been further identified as an additional and unique type of dual-vortex interaction in several recent studies. The interaction between the typhoons Tembin and Bolaven in 2012 was examined, where TDs located between the typhoons resulted in an indirect cyclone−cyclone interaction [18]. Empirical formulas (referred to as Liou−Liu formulas) have been proposed for determining the threshold distance required for substantial interactions between storms [19]. The formulas are empirically based on the size factor (SF), height difference (HD), rotation factor (RF), and current intensity (CI) of TCs, where CI accounts for the maximum wind speed and intensity of TCs. The Liou−Liu formulas have been successfully used to predict and quantify the impacts of intermediate TDs, and these formulas can therefore be applied to modeling of TDs mosaic dual-vortex interactions between two TCs.

Seven typhoon-prone ocean basins have appeared in the NWP, with an average of 24 typhoons formed per year in the last four decades (1977−2016) [20,21]. The influence of cooler air masses, air flows, and outflow jets on typhoons is high in the NWP basin because upper cooler air masses result in a temperature gradient toward the north, whereas lower air flows transfer warm and humid air from the south to the typhoons formed in the NWP. Both the Haiyan and Hagupit typhoons intensified into super-typhoons (STYs) through their interactions with cold fronts in the NWP during the winter seasons of 2013 and 2014 [22]. Occasionally, southwest air flows play a crucial role in intensifying typhoons in the NWP during summer [23]. Better visualization of such influence is essential in the study of typhoon intensification processes in the NWP. Studies have analyzed the influence of the seasonal variations of all seven STYs in 2014 in the NWP on their distribution and profiles [22,24]. The results verified the critical role of northwest cold air masses and southwest air flows in strengthening both winter and summer STYs. Both cold fronts and southwest air flows can increase or decrease the STY intensity in winter. This study investigated how the weather features of southwest air flows and occluded fronts play a vital role in changing the typhoon intensity, such as enhancement and reduction during the STY passage. STY (Nuri) images from the winter of 2014 were analyzed [25].

A recent study of all 30 STYs in 2013−2017 in the NWP showed that each STY is influenced by southwest air flows in summer and by the Siberian-Mongolian high-origination cool air masses in winter [9]. Moreover, on average, winter STYs are stronger than summer STYs in this region because of additional weaker southwest air flows in most STYs in winter. Moreover, the zones in the NWP where STYs are prone to take a turn/curved track or achieve the STY strength level were evaluated season-wise, and the influencing seasonal environmental factors at that time were also identified. It was found that STYs accompanied by southwestern air flows or both southwestern air flows and cooler air masses exhibit a higher degree of interaction than STYs accompanied by other effects [9]. This rise of STYs has also recently been reported under the headline of "Typhoons Getting Stronger, Making Landfall More Often" [26] in the Eos science news magazine. Accordingly, various environmental issues, such as salinity intrusion, which alter weather, and typhoon intensity have been examined using various tools, such as an indicator derived from Landsat 8 OLI data [27].

The observation and quantification of dual-vortex interactions are essential for the efficiency of weather prediction models and forecasts. In a previous study, to validate cyclonic interactions, three successive dual-vortex interactions were studied using the generalized Liou−Liu formulas, which calculate the threshold distances between the centers of two cyclonic systems required for their substantial interactions [28]. These sets of dual-vortex interactions occurred between the typhoons Noru and TS Kulap, typhoons Noru and Nesat, and the jet flows and air flows separating them, as well as between the typhoons Nesat and TD Haitang [28].

This study used a combination of various techniques to analyze the In-Fa and Cempaka typhoons and the surrounding weather patterns during the 2021 typhoon season in the North Pacific; the development of these storm systems and their interactions are summarized below.

At 06:00 UTC on July 14, 2021, a persistent area of convection, associated with a low-level circulation center, was located 895 km west-northwest of Guam. At 00:00 UTC on July 18, the disturbance was upgraded to a depression and was designated TD Fabian. At that time, TD Fabian moved slowly northwestward before turning northward. Later, Fabian became a TS and was assigned the name In-Fa. It developed rapidly over the Philippine Sea and continued its trajectory toward Ryukyu Islands. Typhoon In-Fa began to take a northwest track before moving west-northwestward over Japan by the early hours of July 19. At 00:00 UTC on July 19, In-Fa and intensified to a severe TS. Later, In-Fa became a typhoon located approximately 895 km to the east of extreme Northern Luzon. At the same time, the first curved bending of the track appeared. In-Fa started to move westward with a west-southwest track. At 22:00 UTC on July 19, its 65-km eye was evident on satellite images; then, the eye started to enlarge, and In-Fa was upgraded to a mid-level typhoon at 03:00 UTC on July 21, with winds of 145 km/h. At 20:00 UTC on July 21, satellite images from Okinawa Island showed a marked and clear eye and revealed that the eyewall was moving westward. Later, as it shifted its motion west-southwestward, In-Fa's eye became ragged. At 03:00 UTC on July 22, In-Fa started an eyewall replacement cycle and its northern quadrant started to weaken as it changed its movement yet again to the south-southwest. At 09:00 UTC on July 22, the typhoon started to weaken with its eye expanding and showed curved bending movement while tracking westward-northwestward gradually. Then, a second curved bending movement was caused by a subtropical ridge to the north. At 15:00 UTC on July 23, In-Fa passed between Tarama Island and Miyako-Jima Island, with its eye remaining large as it slightly shifted its movement toward the north-northwest. At 02:00 UTC on July 24, the typhoon further reached its peak with maximum sustained winds of 150 km/h (90 mph) and a minimum barometric pressure of 950 hPa. At 03:00 UTC on July 24, In-Fa reformed its convective depth and maintained a ragged eye while moving northward, and it started to move north-northwestward over the Sea of Japan. At 04:30 UTC on July 26, the system made its first landfall in the city of Zhoushan in the eastern Chinese province of Zhejiang.

Typhoon Cempaka was slowly approaching China's Guangdong Province, and it was expected to make landfall on July 20, 2021. At 00:00 UTC on July 20, satellite imagery revealed that the system had maintained an overall convective signature and exhibited a well-defined, but cloud-filled, eye as it tracked very slowly toward China. At 06:00 UTC on July 20, the center of Cempaka was located approximately 215 km (135 miles) from Hong Kong. It had maximum 10-min duration winds at 100 km/h (62 mph). The minimum central barometric pressure was 992 hPa, and the system was almost stationary. Tracks of the cyclonic systems In-Fa and Cempaka over July 17−27, 2021 are presented in Fig. 1.

During July 19−22, 2021, the centers of the typhoons In-Fa and Cempaka were 1,800−2,040 km apart. Despite the considerable distance between the typhoons, the influence of middle air flows and TD caused vector addition TD-mosaic dual-vortex interactions between these two typhoons, and two mid-TDs could be observed in cloud images. A variety of TD-mosaic dual-vortex interactions, including (a) typical TD-mosaic dual-vortex interaction, (b) offset TD-mosaic dual-vortex interaction, (c) two TD-mosaic dual-vortex interaction, and (d) vector addition TD-mosaic dual-vortex interaction, were observed between In-Fa and Cempaka. These interactions created stronger typhoons with clear eyes of diameters of 25, 50, 65, and 150 km and caused the curved bending (zig-zag) tracks of Typhoon In-Fa and the U-turn track of Typhoon Cempaka.

The Liou−Liu empirical formulas have been successfully applied for quantifying the threshold distance required for interactions between TCs/typhoons and two TDs whenever all phenomena coexist in the North Pacific Ocean. This paper expands the utility of these formulas by applying vector space technology, that is, a vector addition diagram depicting vector addition for TD-mosaic dual-vortex interactions.

2. Liou−Liu formulas and vector addition diagram

2.1. Liou−Liu formulas

The Liou−Liu formulas are applied to quantitatively describe the chance of dual-vortex interactions, potentially improving weather forecasts. Moreover, they can characterize several types of dual-vortex interactions. For any two simultaneously occurring individual cyclones designated TC_1 and TC_2, which have the current intensity (CI) values of CI_1 and CI_2, as obtained from their respective maximum wind speed and intensity, the threshold distance can be calculated. The pressure−wind relationship for intense TCs has been examined [28]; the current intensity focuses on the physical connections between the maximum

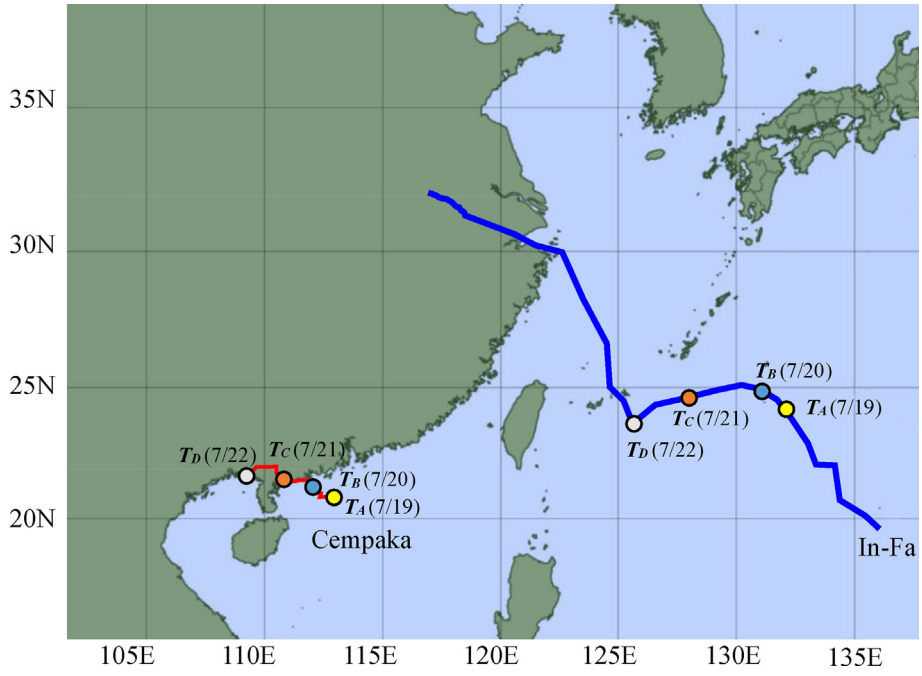

Fig. 1. Tracks of the typhoons In-Fa and Cempaka in the North West Pacific.

surface wind and minimum sea-level pressure. The effects of vortex size, background environmental pressure, and complex vortex features are not addressed in these formulas.

The threshold distance d_{th} (km), which is calculated using the Liou−Liu formulas, determines whether TC_1 and TC_2 experience marked dual-vortex interactions. The first version of the Liou−Liu empirical formulas defined by (1) is applied for the typical dual-vortex interactions as follows:

$$d_{th} = 1000 + 100\left(\frac{CI_1}{4} + \frac{CI_2}{4}\right) \tag{1}$$

For example, in some special situations, a TD or TS occupies the region between two individual cyclone systems. A cyclone's interaction with an intervening TD or TS is unusual and differs from the typical cyclone-to-cyclone interaction. Upward convection may occur between them because a TD or TS is smaller than a cyclone. Such upward convections can strengthen the cyclone and sustain its rotation. Thus, size ratios, height differences, and rotation should be included when calculating threshold distances by using the Liou−Liu formulas under these specific situations. Under such conditions, the Liou−Liu formulas for each threshold distance, d_{th1} and d_{th2}, can determine two sets of dual-vortex interactions that may occur, and these two distances also exist between TC_1 (CI_1) and TD (CI_d) and between TC_2 (CI_2) and TD (CI_d). Hence, a second version of the Liou−Liu formulas defined by (2) is applied for measuring the threshold distance D_{th} to quantitatively determine the TD-mosaic dual-vortex interaction, as follows:

$$\begin{aligned} D_{th} = d_{th1} + d_{th2} = 2000 &+ 100\left(\frac{CI_1}{4} + \frac{CI_d}{4}\right)F_1 \\ &+ 100\left(\frac{CI_2}{4} + \frac{CI_d}{4}\right)F_2 \end{aligned} \tag{2}$$

where F_1 and F_2 are the tuning factors dependent on size, relative height difference, and rotation factors. For simplification, take $F_1 = F_2 = 1$.

Generalized dual-vortex interactions that involve typical dual-vortex interactions and TD-mosaic dual-vortex interactions have been introduced in previous studies [19,28], in which the Liou−Liu formulas could successfully predict these interactions and quantified the impacts of intermediate TDs on the interactions. In the first case [19], the typical dual-vortex interactions between the typhoons In-Fa and Cempaka were analyzed using Eq. (1), and in the second case [28], the TD-mosaic dual-vortex interactions with one TD/TS among typhoons/TCs were analyzed using Eq. (2).

2.2. Variety of TD-mosaic dual-vortex interactions

The variety of TD-mosaic dual-vortex interactions observed between the typhoons In-Fa and Cempaka included single TD-mosaic dual-vortex interaction, offset TD-mosaic dual-vortex interaction, double

TD-mosaic dual-vortex interaction, and vector addition TD-mosaic dual-vortex interaction. The single TD-mosaic dual-vortex interaction is depicted in Fig. 2(a), where TC_1, TD, and TC_2 are located on a line; the TD-mosaic interaction is located between the two TCs, and two sets of TC−TD interactions exist, which cause indirect cyclone−cyclone interaction. The offset TD-mosaic dual-vortex interaction is shown in Fig. 2(b). The indirect cyclone−cyclone interaction possibly occurs through the two sets of depression−cyclone interactions and is related to the distance between TC_1 and TC_2; the offset distance (o) fits the assumption of $o < d/3$. The double TD-mosaic dual-vortex interaction is presented in Fig. 2(c). The indirect cyclone−cyclone interaction possibly results from the two sets of depression−cyclone interactions and the subsequent merging of TD_1 and TD_2, and the space between TD_1 and TD_2 fits the assumption of $s < d/3$. The vector addition TD-mosaic dual-vortex interaction is illustrated in Fig. 2(d). The neighboring southwest air flow (s_1 and s_2) between TC_1 and TC_2 occurs, which consists of two branched air flows (with lengths of s_1 [TD_{01} to TD_0] and s_2 [TD_{02} to TD_0]) connected with a vertex (TD_0). The TD-mosaic interaction is located between the two TCs, and two sets of TC−TDs interactions exist, which also causes indirect cyclone−cyclone interaction. When this TD-mosaic cyclone−cyclone interaction occurs, the interaction among "TD_{01} to TD_0" and "TD_{02} to TD_0" encompasses vector (linear) spaces, wherein vector spaces (u and w) specify the independent directions in space. Vector addition indicates that vector u is added to vector w, yielding the sum $u + w$. In the various TD-mosaic dual-vortex interactions shown in Fig. 2(a)−(d), the TD-mosaic dual-vortex interactions with TDs among typhoons TCs were analyzed using Eq. (2).

3. TD-mosaic dual-vortex interactions between In-Fa and Cempaka (2021)

The Himawari-8 geostationary weather satellite images of thermal infrared band 1 (3.9 μm) at 10-min intervals were collected for this current study [20]. The whole dataset combines vast amounts of historical observations into global estimates using advanced modeling and data assimilation systems and is provided freely for public use through the online link: https://www.ecmwf.int/en/forecasts/datasets/reanalysis-datasets/era5.

The tracks of the cyclonic systems In-Fa and Cempaka over July 17−27, 2021 are presented in Fig. 1. From 09:00 UTC on 19 July to 09:00 UTC on 22 July, obvious changes occurred in the zig-zag track of Typhoon In-Fa and the U-turn track of Typhoon Cempaka. The four time intervals of T_A = 09:00 UTC on 19 July, T_B = 09:00 UTC on 20 July, T_C = 09:00 UTC on 21 July, and T_D = 09:00 UTC on 22 July were chosen for this study. Based on the four cloud images presented in Fig. 3, the threshold distances for the interaction between In-Fa and Cempaka were determined over the four intervals. For the typical dual-vortex interaction, the threshold distances were calculated using Eq. (1). No dual-vortex interactions occurred in the four intervals because the measured distances (2,040, 1,920, 1,910, and 1,800 km) between the two typhoons were larger

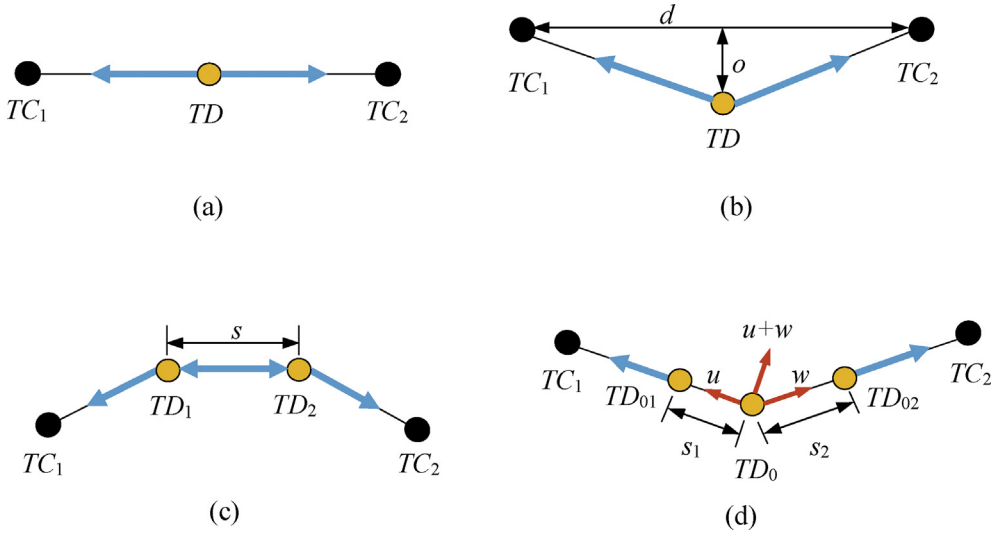

Fig. 2. Variety of TD-mosaic dual-vortex interactions. (a) Single TD-mosaic dual-vortex interaction, (b) Offset TD-mosaic dual-vortex interaction, (c) Double TD-mosaic dual-vortex interaction, and (d) Vector addition TD-mosaic dual-vortex interaction.

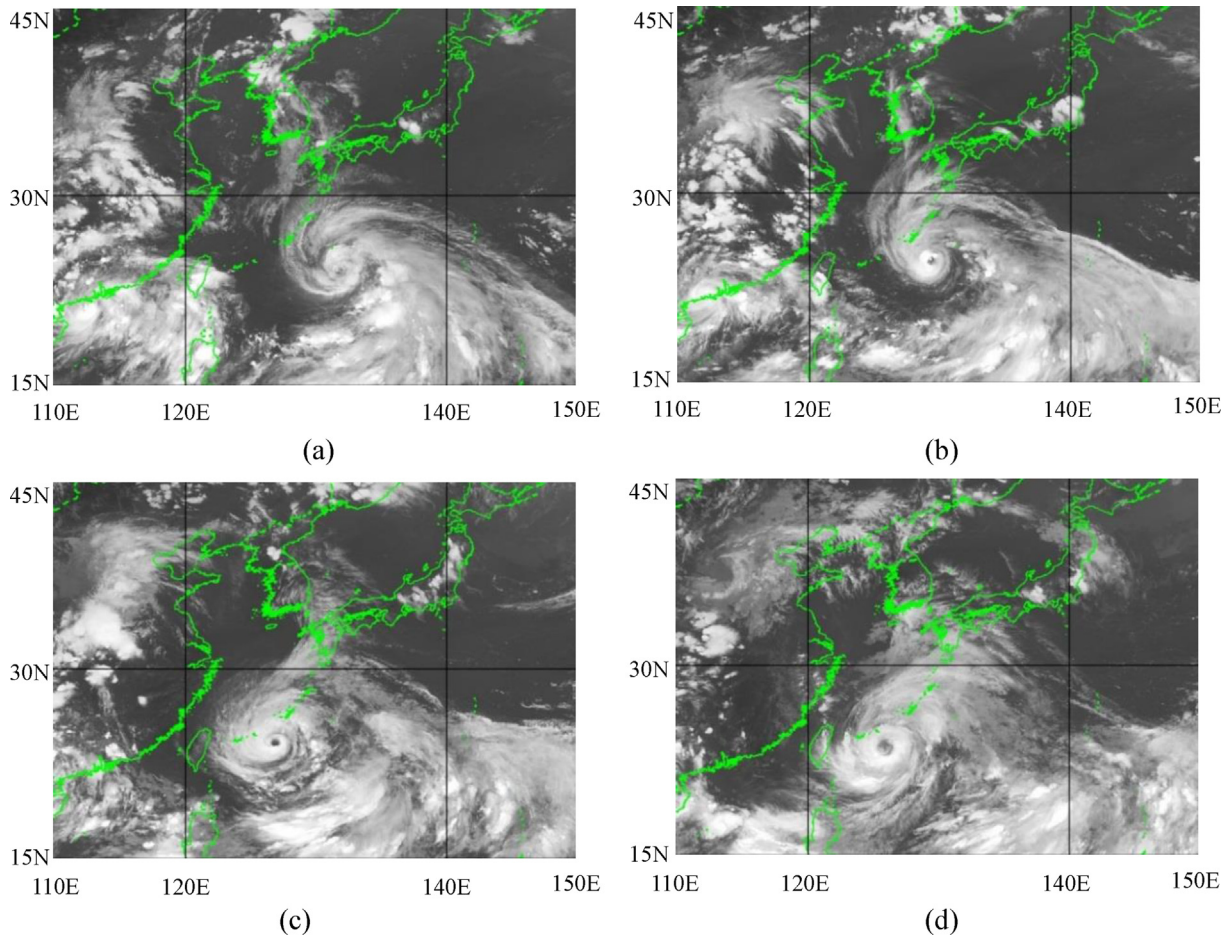

Fig. 3. Four cloud images for this study. (a) at T_A = 09:00 UTC on 19 July, (b) at T_B = 09:00 UTC on 20 July, (c) at T_C = 09:00 on 21 July, and (d) at T_D = 09:00 UTC on 22 July.

than the calculated threshold distances (1,130, 1,170, 1,180, and 1,160). All the values are presented in Table 1.

For the TD-mosaic dual-vortex interaction, the threshold distances were calculated using Eq. (2), substituting $F_1 = F_2 = 1$ for approximations. At the T_A time interval, the value of $CI_{d1,2}$ was 1.4 for $TD_{1,2}$ (unclassified TDs at N29°N/127°E and 28°N/123°E), and the value of $CI_{d01,02}$ was 2.4 for $TD_{01,02}$ (unclassified TDs at 22°N/116°E and 21°N/136°E). At T_B, T_C, and T_D time intervals, the values of CI_d were 1.2, 1.2, and 1.6 for TD (unclassified TDs at N23°N/118°E, N21.5°N/115°E, and 17°N/119°E). All the values are listed in Table 2. Several techniques incorporate the

Table 1. Prediction of dual-vertex by using Eq 1

	T_A: 7/19 09:00 UTC	T_B: 7/20 09:00 UTC	T_C: 7/21 09:00 UTC	T_D: 7/22 09:00 UTC
TC_1: In-Fa pressure (hPa)	990	985	965	955
CI_1 value	2.7	3.2	4.5	5.1
TC_1: Position	25°N	25°N	24°N	23.5°N
	132°E	131°E	128°E	126°E
TC_2: Cempaka pressure (hPa)	992	977	990	1,000
CI_2 value	2.5	3.8	2.7	1.4
TC_2: Position	21°N	22°N	20.5°N	20°N
	112.5°E	112.5°E	110°E	109°E
Measured distance between In-Fa and Cempaka (d, km)	2,040	1,920	1,910	1,800
Calculated threshold distance by Eq. (1) (d_{th}, km)	1,130	1,175	1,180	1.170
Dual-vertex interaction	No	No	No	No

Table 2. Prediction of dual-vertex by using Eq 2

	T_A: 7/19 09:00 UTC	T_B: 7/20 09:00 UTC	T_C: 7/21 09:00 UTC	T_D: 7/22 09:00 UTC
TC_1: In-Fa pressure (hPa)	990	985	965	955
CI_1 value	2.7	3.2	4.5	5.1
TC_2: Cempaka pressure (hPa)	992	977	990	1,000
CI_2 value	2.5	3.8	2.7	1.4
CI_{d1}, CI_{d2} value	1.4	–	–	–
CI_{d01}, CI_{d02} value	2.4	–	–	–
CI_d value		1.2	1.2	1.6
Measured distance between In-Fa and TD_1, Cempaka and TD_1 (d, km)	666 1,316 (1,982)	–	–	–
Measured distance between In-Fa and TD_2, Cempaka and TD_2 (d, km)		–	–	–
Measured distance between In-Fa and TD_{01}, Cempaka and TD_{02} (d, km)	604 379 (983)			
Measured distance between In-Fa and TD, Cempaka and TD (d, km)		1,338 576 (1,914)	1,411 480 (1,891)	1,027 1,106 (2,133)
Calculated threshold distance by 2nd formula (d_{th2}, km)	2,200 2,250	2,235	2,200	2,243
Dual-vertex interaction	Type A	Type B	Type B	Type C
Behavior	*I	*II	*III	*IV

Types of dual-vertex interaction: Type A: two TD-mosaic and vector addition TD-mosaic dual-vortex interactions, Type B: typical TD-mosaic dual-vortex interaction, and Type C: offset TD-mosaic dual-vortex interaction.
*I: In-Fa changed direction with first curved bending, Cempaka changed direction with a U-turn.
*II: Dual-vortex interactions existed between In-Fa and Cempaka; both In-Fa and Cempaka strengthened.
*III: Dual-vortex interactions existed between In-Fa and Cempaka; In-Fa continuously strengthened.
*IV: In-Fa changed direction with a second curved bending and continuously strengthened; Cempaka changed direction with a U-turn.

relationships between CI number and minimum sea-level pressure or maximum wind speed of TCs [29]. The wave number-one perturbation technique [30] and the maximum vertical values of radar reflectivity with geopotential height [31] have been proposed to obtain alternative values of F_1 and F_2.

During the first to fourth intervals, TD-mosaic dual-vortex interactions were present because the measured distances (1,982/983, 1,914, 1,891, and 2,133 km) between the two typhoons and TD were less than the calculated threshold distances (2,200/2,350, 2,235, 2,200, and 2,243 km). Thus, TD-mosaic dual-vortex interactions were present in the four intervals. Regarding typhoon behaviors in the first interval, In-Fa changed direction with the first curved bending, and Cempaka changed direction with a U-turn. In the second interval, a dual-vertex interaction between In-Fa and Cempaka was noted, and both typhoons became stronger. In the third interval, a dual-vertex interaction between In-Fa and Cempaka was noted, and the typhoons continuously strengthened. In the fourth interval, In-Fa changed direction with a second curved bending and continued to strengthen, and Cempaka changed direction with a U-turn.

Figures 4(a)−4(c), 5, 6, and 7(a)−(f) all clarify the various TD-mosaic dual-vortex interactions. Double TD-mosaic dual-vortex interaction and vector addition TD-mosaic dual-vortex interactions were analyzed based on the cloud images for July 19 at 07:10 in Fig. 4(a)−(c). Figure 4(a) provides the TIR image, Fig. 4(b) presents the temperature distribution image, and Fig. 4(c) provides the height distribution image. The temperature and height distribution images were obtained through linear interpolation based on the grayscale of the original cloud image. According to the definition of the Himawari-8 satellite cloud image, 200 K is represented by grayscale white (255), and 330 K is represented by black (0). Therefore, the relationship between the image pixel grayscale and the corresponding Celsius temperature is expressed as

$$temperature(x,y) = 56.85 - \frac{130}{255}p(x,y) \tag{3}$$

where $p(x, y)$ is the grayscale of the pixels at the position (x, y) on the satellite cloud image. For displaying the height distribution of the original cloud image in this paper, the sea level (altitude is 0 m) is set at the reference temperature of 20 °C, and the changing basis is a temperature drop of 0.65 °C at a height of 100 m. The resulting height distribution is defined as

$$height(x,y) = \frac{20 - temperature(x,y)}{0.65} \cdot 100 \tag{4}$$

The method of finding the double TDs with dual-typhoons is illustrated in Fig. 2(c), and (d) presents VAL, which clearly appears in the images

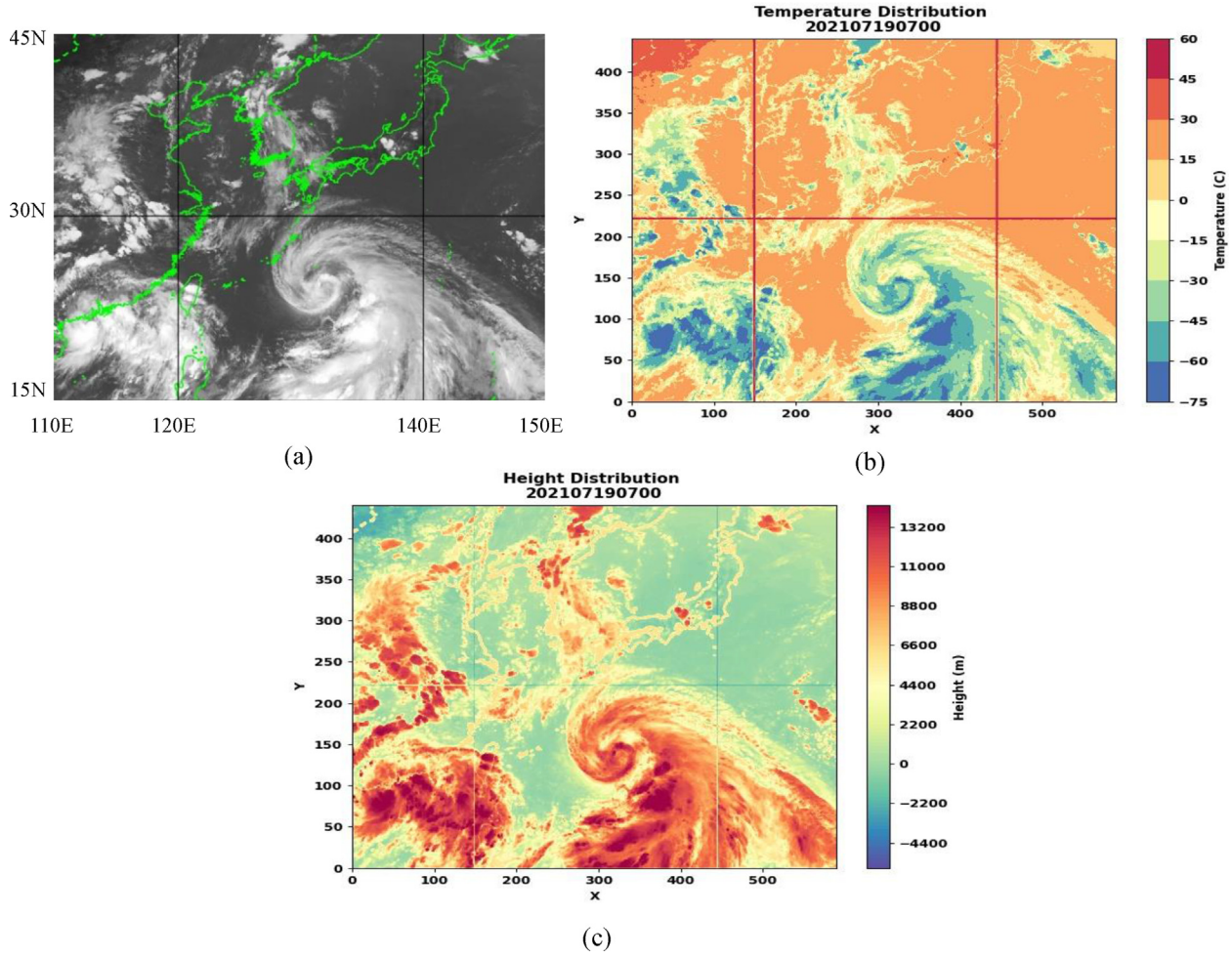

Fig. 4. Cloud images at T_1 = 07:00 on 19 July. (a) TIR image. (b) Temperature distribution. and (c) Height distribution.

of Figs. 3(a) and 4(a) and (c). Moreover, the existence of VAL among two TDs and dual-typhoons was identified in the 3-h interval from 07:00 to 10:00 UTC on 19 July. During the VAL interval, the strengthening of Typhoon In-Fa occurred. The vector addition TD-mosaic dual-vortex interaction is shown in Fig. 2(d). The positions of TC_1, TC_2, and TDs are presented in Table 3. In addition to TC_1 and TC_2, the neighboring southwest air flow is present, which consists of two branched air flows (with lengths of s_1 [TD_{01} to TD_0] and s_2 [TD_{02} to TD_0]) connected with a vertex (TD_0). s_1 represents a vector u, and s_2 denotes vector w. For such vectors u and w, the parallelogram spanned by them contains one diagonal vector that starts at the origin. This new vector (diagonal) is the sum of the two vectors and is denoted $u + w$.

To elucidate the various single TD-mosaic dual-vortex interactions, the cloud images at 22:00 UTC on July 19 and at 00:00 UTC on July 20 are provided in Figs. 5 and 7(a) and (b), respectively. The cloud images at 20:00 UTC on July 21, at 10:00 UTC on July 22, at 23:00 on July 23, and at 09:00 on July 24 in Figs. 5 and 7(c), (d), (e), and (f), respectively, display the various offset TD-mosaic dual-vortex interactions.

The eye pattern is an interesting feature of typhoons. In Figs. 5, 6, 7, the aforementioned interactions led to the strengthening of In-Fa and Cempaka with clear eyes of diameters 25, 55, 60, 65, 75, and 100 km. First, at 22:00 UTC on July 19 and at 00:00 UTC on July 20, Typhoon In-Fa had eyes (990/985 hPb) with diameters of 55/60 km, and Typhoon Cempaka had tiny eyes (985/975 hPb) with diameters of 25/25 km, as shown in Figs. 6 and 7(a) and (b), respectively. Second, at 20:00 UTC on July 21 and at 10:00 UTC on July 22, Typhoon In-Fa exhibited whole eyes (955/955 hPb) with diameters of 65/75 km, and an eye-wall with an aperture of −/175 km was found for Typhoon Cempaka, as shown in Figs. 6 and 7(c) and (d), respectively. Third, at 23:00 on July 23, Typhoon In-Fa had a bigger eye (960 hPb) with a diameter of 100 km, and Typhoon

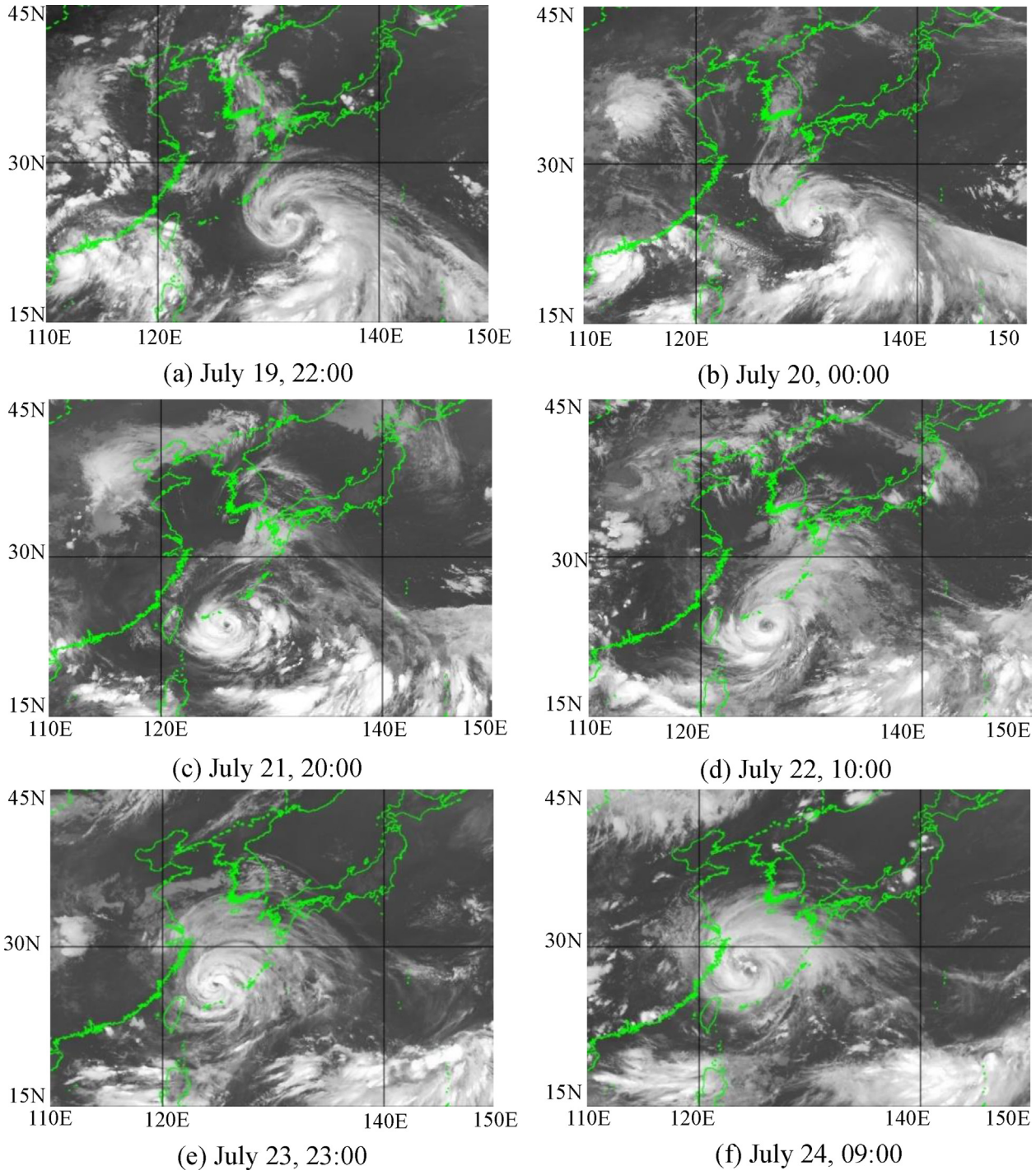

Fig. 5. TIR images.

Cempaka had an eye-wall with an aperture of 165 km, as illustrated in Figs. 6 and 7(e). Finally, at 09:00 on July 24, the whole eye (low pressure of 950 hPb) with a diameter of 55 km was present in Typhoon In-Fa, as shown in Figs. 6 and 7(f). The diverse eyes with various diameters are tabulated in Table 4.

4. Applications

For applications, a typhoon forecasting procedure is proposed as follows:

Step 1:

When two typhoons exist simultaneously, the empirical Liou−Liu formulas (1) are used to

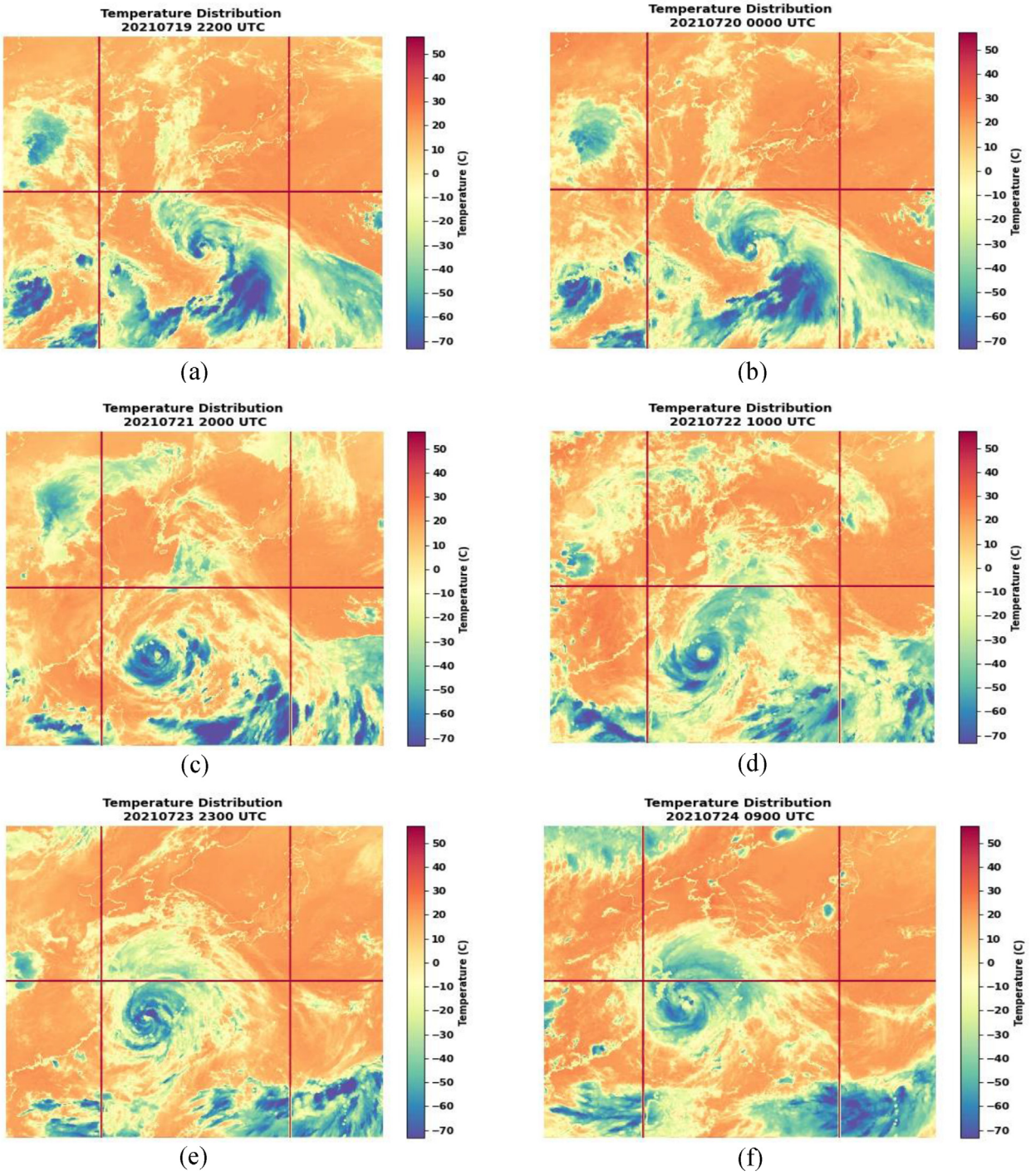

Fig. 6. Temperature distribution images (a) at 22:00 on July 19, (b) at 00:00 on July 20, (c) at 20:00 on July 21, (d) at 10:00 on July 22, (e) at 23:00 on July 23, and (f) at 09:00 on July 24.

calculate the threshold distance for the interaction between two TCs with their respective CI numbers for determining the possibility of marked dual-vortex interactions. When the threshold distance for the interaction is higher than the actual measured distance between the centers of two typhoons, dual-vortex interactions are confirmed to occur.

Dual-vortex interactions are frequently associated with increased typhoon track sinuosity through changes in the track direction and the execution of complex/looping tracks. Occasionally, typhoons make U-turns with increasing intensity. As a result, several potential dual-vortex interactions, such as CM, PM, CSO, PSO, and EI, occur.

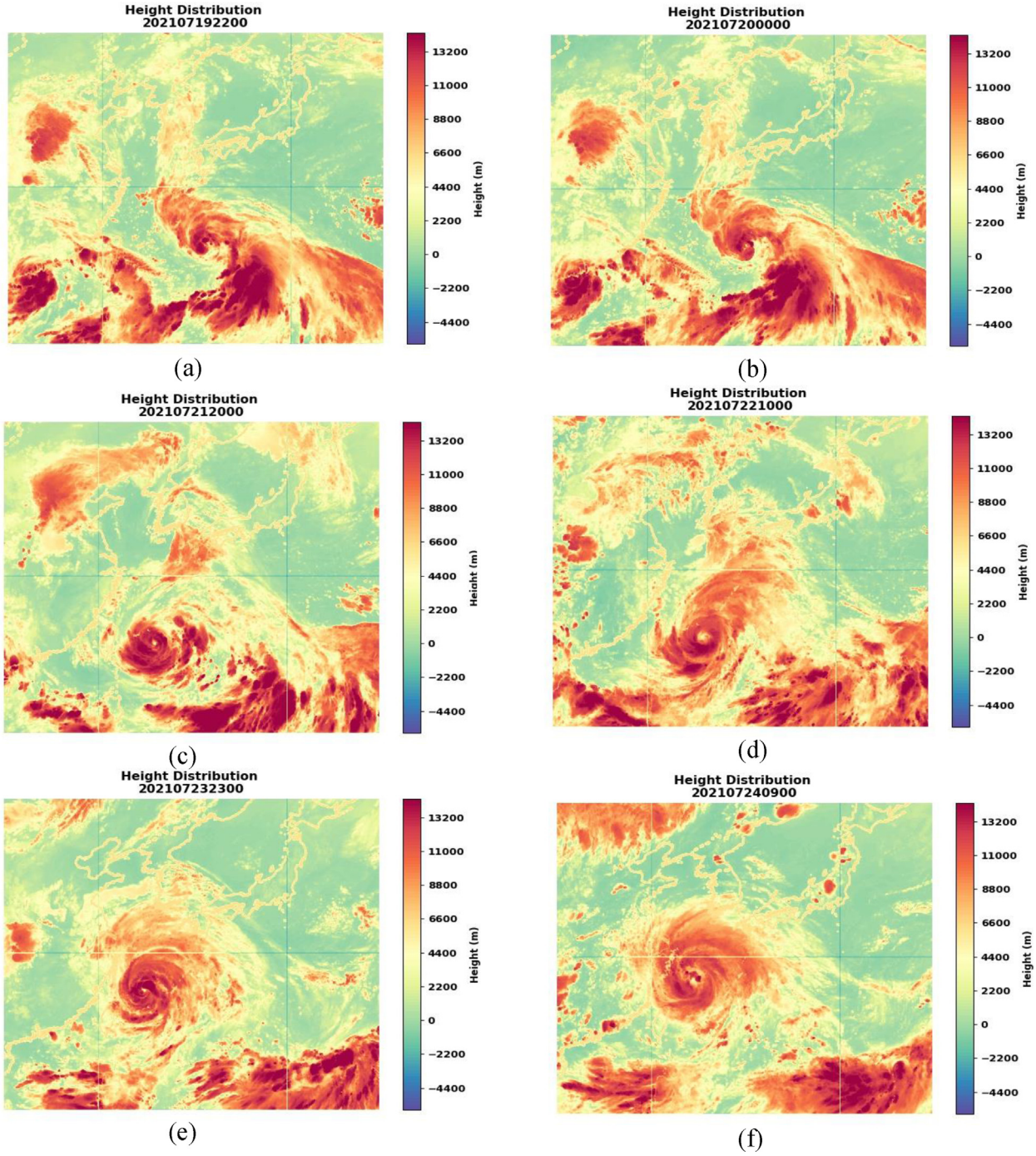

Fig. 7. Height distribution images (a) at 22:00 UTC on July 19, (b) at 00:00 UTC on July 20, (c) at 20:00 UTC on July 21, (d) at 10:00 UTC on July 22, (e) at 23:00 on July 23, and (f) at 09:00 on July 24.

Step 2:

When two typhoons with single TD-mosaic vortices exist simultaneously, the empirical Liou−Liu formulas (2) are used to calculate threshold distances for interactions between TC and TD/TS related to the CI number, size factor, height difference, and rotation factor for determining whether dual-vortex interactions occur. When threshold distances for interactions are higher than the measured distances between the centers of both typhoons and TD, dual-vortex interactions are confirmed to occur.

Table 3. Positions of TC_1, TC_2, and TDs

	T_A: 7/19 09:00 UTC	T_B: 7/20 09:00 UTC	T_C: 7/21 09:00 UTC	T_D: 7/22 09:00 UTC
TC_1: Position	25^{0}N 132^{0}E 21^{0}N 136^{0}E	25°N 131°E	24°N 128°E	23.5°N 126°E
TC_2: Position	21^{0}N 112.5^{0}E 22^{0}N 116^{0}E	22^{0}N 112.5^{0}E	20.5^{0}N 110^{0}E	20^{0}N 109^{0}E
TD_1: Position	29^{0}N 127^{0}E	–	–	–
TD_2: Position	28^{0}N 123^{0}E	–	–	–
TD_{01}: Position	22^{0}N 116^{0}E	–	–	–
TD_0: Position	17^{0}N 125^{0}E	–	–	–
TD_{02}: Position	21^{0}N 136^{0}E	–	–	–
TD: Position		23^{0}N 118^{0}E	21.5^{0}N 115^{0}E	17^{0}N 119^{0}E

Table 4. Eye patterns

Typhoon	Performance	7/19 22:00	7/20 00:00	7/21 20:00	7/22 10:00	7/23 23:00	7/24 09:00
In-Fa	Pressure (hPb)	990	985	955	955	960	950
In-Fa	Eye diameter (km)	55	60	65	75	100	55
In-Fa	Eye-wall aperture (km)	–	–	–	175	165	–
Cempaka	Pressure (hPb)	985	975	–	–	–	–
Cempaka	Eye diameter (km)	25	25	–	–	–	–

Step 3:

When two typhoons with offset TD-mosaic vortices exist simultaneously, indirect cyclone−cyclone interaction may occur through two sets of depression−cyclone interactions and is related to the distance between TC_1 and TC_2; the offset distance (o) fits the assumption of $o < d/3$. The empirical Liou−Liu formulas (2) are used to estimate threshold distances for interactions between TC and TD related to the CI number, size factor, height difference, and rotation factor for determining whether dual-vortex interactions occur. Dual-vortex interactions are confirmed to occur when the threshold distances for interactions are higher than the actual measured distances between the two typhoons and TD centers.

Step 4:

When two typhoons with double TD-mosaic vortices exist simultaneously, indirect cyclone−cyclone interactions may occur through the two sets of depression−cyclone interactions and the subsequent merging of TD_1 and TD_2, and the space (s) between TD_1 and TD_2 fits the assumption of $s < d/3$. The empirical Liou−Liu formulas (2) are used to calculate threshold distances for interactions between two TCs and two TDs related to the CI number, size factor, height difference, and rotation factor for determining whether dual-vortex interactions occur. When the threshold distances for interactions are higher than the actual measured distances between the centers of the two typhoons and TDs, dual-vortex interactions are confirmed to occur.

Step 5:

When mid-southwest air flows are located between two TCs, vector addition TD-mosaic vortices exist, and two sets of TC−TD interactions occur, causing indirect cyclone−cyclone interactions. This type of TD-mosaic cyclone−cyclone interaction is termed as vector addition TD-mosaic double-vortex interaction.

5. Conclusion

In this paper, the various TD-mosaic dual-vortex interactions include (a) simple TD-mosaic dual-vortex interaction, (b) offset TD-mosaic dual-vortex interaction, (c) double TD-mosaic dual-vortex interaction, and (d) vector addition TD-mosaic dual-

vortex interaction. They are observed in addition to the early known conventional patterns of dual-vortex interactions between TCs, such as CM, PM, CSO, PSO, and EI. Despite the enormous distance (2,050−2,150 km) between the respective centers of the typhoons In-Fa and Cempaka, the influence of middle air flows and a TD caused TD-mosaic dual-vortex interactions between these typhoons.

The Liou−Liu empirical formulas have been successfully used for quantifying the threshold distance for interactions between TCs/typhoons and two TDs whenever all phenomena co-exist in the North Pacific Ocean. Linear (vector) space technology, that is, the vector addition diagram, is used to depict the vector addition TD-mosaic dual-vortex interaction among all TCs and TDs. For the first time, the existence of VAL between two TDs and dual typhoons was identified, in this case, during the 3-h time interval from 07:00 to 10:00 on 19 July. During the VAL interval, the strengthening of Typhoon In-Fa occurred.

One interesting feature of typhoons is the eye pattern resulting from the TD-mosaic dual-vortex interaction. Temperature and height distribution techniques are proposed for applying versatile images exhibiting eyes of various diameters. The aforementioned interactions lead to stronger typhoons with clear eyes of diameters 20, 25, 55, 60, 65, 75, and 100 km, diverting the movement to the zigzag track of Typhoon In-Fa and the U-turn track of Typhoon Cempaka. This research provides a practical application in the form of a proposed typhoon forecasting procedure in cases of diverse conditions of dual-vortex interactions.

Declaration of competing interest

There was no conflict of interest.

Acknowledgment

This work was supported in part by the Ministry of Science and Technology (MOST), through MOST grant 110-2221-E-130-006.

References

[1] Lin CY, Hsu HM, Sheng YF, Kuo CH Kuo, Liou YA. Mesoscale processes for super heavy rainfall of typhoon Morakot (2009) over southern Taiwan. Atmos Chem Phys 2011;11:345−61.
[2] Terry JP, Kim I-H, Jolivet S. Sinuosity of tropical cyclone tracks in the South West Indian Ocean: spatio-temporal patterns and relationships with fundamental storm attributes. Appl Geogr 2013;45:29−40.
[3] Terry JP, Kim I-H. Morphometric analysis of tropical storm and hurricane tracks in the North Atlantic basin using a sinuosity-based approach. Int J Climatol 2015;35:923−34.
[4] Piñeros MF, Ritchie EA, Tyo JS. Objective measures of tropical cyclone structure and intensity change from remotely sensed infrared image data. IEEE Trans Geosci Rem Sens 2008;46(11):3574−80.
[5] Chang PL, Jou BJD, Zhang J. An algorithm for tracking eyes of tropical cyclones Weather and Forecasting. 2009. p. 245−61. 24.
[6] Wimmers AJ, Velden CS. Objectively determining the rotational center of tropical cyclones in passive microwave satellite imagery. J Appl Meteorol Climatol 2010;49:2013−34.
[7] Wimmers AJ, Velden CS. Advancements in objective multisatellite tropical cyclone center fixing. J Appl Meteorol Climatol 2016;55(1):197−212.
[8] Liou YA, Liu JC, Chane-Ming F, Hong JS, Huang CY, Chiang PK, et al. Remote sensing for improved forecast of typhoons. In: Remote sensing of the Asian seas. Cham: Springer; 2019. p. 251−67.
[9] Pandey RS, Liou YA, Liu JC. Season-dependent variability and influential environmental factors of super-typhoons in the Northwest Pacific basin during 2013-2017. Weather Clim Extrem 2021;31:100307.
[10] Fujiwhara S. The natural tendency towards symmetry of motion and its application as a principle in meteorology. Quar J Roy Meteoro Soc 1921;47:287−93.
[11] Fujiwhara S. On the growth and decay of vortical systems. Quar J Roy Meteoro Soc 1923;49:75−104.
[12] Liou YA, Pandey RS. Interactions between typhoons Parma and Melor (2009). In: North West Pacific ocean. Weather and climate extremes, vol. 29; 2020. p. 100272.
[13] Prieto R, McNoldy BD, Fulton SR, Schubert WA. A classification of binary tropical cyclone-like vortex interactions. Mon Weather Rev 2003;131:2656−66.
[14] Liu CC, Shyu TY, Chao CC, Lin YF. Analysis on typhoon Long Wang intensity changes over the ocean via satellite data. J Mar Sci Technol 2009;17(1):23−8.
[15] Zhang CJ, Wang XD. Typhoon cloud image enhancement and reducing speckle with genetic algorithm in stationary wavelet domain. IET Image Process 2009;3(4):200−16.
[16] Hart R, Evans J. Simulations of dual-vortex interaction within environmental shear. J Atmos Sci 1999;56(21):3605−21.
[17] Galarneau JT, Davis CA, Shapiro MA. Intensification of hurricane sandy (2012) through extratropical warm core seclusion. Mon Weather Rev 2013;141:4296−321.
[18] Liu JC, Liou YA, Wu MX, Lee YJ, Cheng CH, Kuei CP, et al. Interactions among two tropical depressions and typhoons Tembin and Bolaven (2012) in the Pacific Ocean: analysis of the depression-cyclone interactions with 3-D reconstruction of satellite cloud images. IEEE Trans Geosci Rem Sens 2015;53(3):1394−402.
[19] Liou YA, Liu JC, Wu MX, Lee YJ, Cheng CH, Kuei CP, et al. Generalized empirical formulas of threshold distance to characterize cyclone-cyclone. IEEE Trans Geosci Rem Sens 2016;54(6):3502−12.
[20] Pandey RS, Liou YA. Decadal behaviors of tropical storm tracks in the North West Pacific ocean. Atmos Res 2020;246:105143.
[21] Pandey RS, Liou YA. Refined and improved tropical storm 6-hourly data and track sinuosity measurements for the North West Pacific basin during 1977-2016. Mendeley Data 2020;31:100307.
[22] Lee YS, Liou YA, Liu JC, Chiang CT, Yeh KD. Formation of winter super-typhoons Haiyan (2013) and Hagupit (2014) through interactions with cold fronts as observed by multifunctional transport satellite. IEEE Trans Geosci Rem Sens 2017;55(7):3800−9.
[23] Jaiswal N, Kishtawal CM. Objective detection of center of tropical cyclone in remotely sensed infrared images. IEEE J Sel Top Appl Earth Obs Rem Sens 2013;6(2):1031−5.
[24] Liou YA, Liu JC, Liu CP, Liu CC. Season-dependent distributions and profiles of seven super-typhoons (2014) in the Northwestern Pacific Ocean from satellite cloud images.

IEEE Trans Geosci Rem Sens 2018;56(5):2949−57. https://doi.org/10.1109/TGRS.2017.2787606.
[25] Yel KD, Liu JC, Eea CM, Lin CH, Lu WL. Intensification and decay of typhoon Nuri (2014) associated with cold front and southwesterly airflow observed in satellite cloud images. J Mar Sci Technol 2017;25(5):599−606.
[26] Hornyak T. Typhoons getting stronger, making landfall more often. Eos 2020;101. https://doi.org/10.1029/2020EO147989. Published on 12 August 2020.
[27] Nguyen KA, Liou YA, Tran PH, Hoang PP, Nguyen TH. Soil salinity assessment by using an indicator derived from Landsat 8 OLI data: a case study in the Tra Vinh Province, Mekong Delta, Vietnam. Prog Earth Planet Sci 2020;7(1): 1−16.
[28] Liou YA, Liu JC, Liu CC, Chen CH, Nguyen KA, Terry JP. Consecutive dual-vortex interactions among quadruple typhoons Noru, Kulap, Nesat and Haitang during the 2017 typhoon season. Rem Sens 2019;11:1843.
[29] Koba H, Hagiwara T, Asano S, Akashi S. Relationships between CI number from Dvorak's technique and minimum sea level pressure or maximum wind speed of tropical cyclone. J Meteorolog Res 1990;42:59−67.
[30] Nolan DS, Montgomery MT, Grasso LD. The wavenumber-one instability and trochoidal motion of hurricane-like vortices. J Atmosph Sci. 2001;58:3243−70.
[31] Jian G, Wu C. A numerical study of the track deflection of super typhoon Haitang (2005) prior to its landfall in Taiwan. Mon Weather Rev 2008;136:598−615.